Interaction-Aware Optimal Safe Speed Control for Autonomous Vehicles Approaching Unsignalized Crosswalks With Pedestrians

Branimir Škugor, *Member, IEEE*, Jakov Topić, Joško Deur, *Senior Member, IEEE*, Vladimir Ivanovic, and H. Eric Tseng

***Abstract*—The proposed autonomous vehicle (AV) safe speed strategy is based on a scenario- and grid-based stochastic model predictive control (SMPC) and a probabilistic neural network (NN) model aimed to predict pedestrian behavior when approaching unsignalized crosswalk. The SMPC problem is formulated to minimize the vehicle traveling time, while accounting for vehicle-pedestrian interaction and keeping the risk of collision with pedestrian low. The vehicle control trajectory is conveniently described by only two parameters to be optimized: the vehicle acceleration and the target speed. Apart from reducing the computational complexity, this simplification facilitates the NN prediction model design in terms of lowering the number of model inputs. The proposed SMPC strategy is verified against a baseline control strategy by means of large-scale stochastic simulations. The verification results indicate that the SMPC strategy on average results in significantly lower vehicle traveling time and less aggressive decelerations, while avoiding pedestrian collisions.**

***Index Terms*—Autonomous vehicles (AVs), neural network (NN), pedestrians, prediction, safety, stochastic model predictive control (SMPC).**

I. Introduction

TO ENABLE the effective and safe operation of autonomous vehicles (AVs) in complex urban environments, interactions with vulnerable road users (VRUs) such as pedestrians attempting to surpass unsignalized crosswalks should be accounted for through proper prediction and control strategies. While human drivers are successful in achieving those tasks, pedestrian behavior prediction, and related vehicle controls represent a challenging problem for AVs [1]. Too conservative driving while confronting pedestrians would lead to long vehicle traveling time, as well as driving discomfort caused by frequent decelerations. On the other hand, too-aggressive driving involves safety risks, including potential collisions with pedestrians. This calls for the design of sophisticated AV control systems that would ensure effective, comfortable, and safe driving in interaction with pedestrians.

While current pedestrian protection systems used in advanced driver assistance systems typically rely on short-term predictions of their upcoming actions (e.g., from a couple of milliseconds to several hundred milliseconds [2], or up to 2.5 s according to [3] and [4]), methods investigated in recent publications mostly deal with longer prediction horizons to achieve safer and more comfortable driving [2] (e.g., 5 s in [5]). Various approaches have been proposed, ranging from rule- to optimization-based ones. For instance, Kapania et al. [6] proposed a rule-based safe speed control strategy which operates according to several modes, i.e., driving, yielding, hard braking, and speed up, depending on the pedestrian's speed and position relative to the crosswalk. Shalev-Shwartz et al. [7] proposed a more general rule-based framework in support of safety assurance standardization. A simple rule-based control strategy for preventing collisions in situations where pedestrians enter the crosswalk from the occluded area is presented in [8], where the vehicle's safe minimum distance and related maximum speed are calculated based on the pedestrian's time-to-arrival to the virtual conflict point. While rule-based approaches are typically simple to implement, they are generally suboptimal (too conservative) and rely only on the current pedestrian state or rough predictions of pedestrian future states.

On the other hand, optimization-based approaches typically incorporate some sort of pedestrian behavior prediction. Prediction models applied in the literature mostly neglect vehicle-pedestrian interaction in terms of vehicle impact on the pedestrian crossing behavior. For instance, the safe speed control strategy proposed in [9] is based on a scenario-based stochastic model predictive control (SMPC), where the pedestrian crossing behavior is predicted via different potential movement trajectories obtained from various constant velocity and constant turn models unified through interacting multiple model Kalman filter, while neglecting the vehicle impact effect. Similarly, a Kalman filter is used in [10] under the constant pedestrian speed assumption to predict the pedestrian trajectory for MPC. The trajectory in [11] is based on the unicycle model, which follows an assumed (predefined) reference under closed-loop control, thus also seemingly having the interaction-unaware character. Another example is given in [12], where MPC is used as a part of the hierarchical path planning framework, and a neural network (NN) is employed

Received 14 August 2024; revised 7 February 2025; accepted 5 April 2025. Date of publication 7 May 2025; date of current version 20 August 2025. This work was supported by Ford Motor Company through University Research Program. Recommended by Associate Editor U. V. Kalabic. *(Corresponding author: Branimir Škugor.)*

Branimir Škugor, Jakov Topić, and Joško Deur are with the Faculty of Mechanical Engineering and Naval Architecture, University of Zagreb, 10002 Zagreb, Croatia (e-mail: branimir.skugor@fsb.unizg.hr; jakov.topic@fsb.unizg.hr; josko.deur@fsb.unizg.hr).

Vladimir Ivanovic is with Ford Research and Advanced Engineering, Dearborn, MI 48124 USA (e-mail: vivanovi@ford.com).

H. Eric Tseng is with the Department of Electrical Engineering, The University of Texas at Arlington, Arlington, TX 76019 USA (e-mail: hongtei.tseng@uta.edu).

Digital Object Identifier 10.1109/TCST.2025.3561056

1063-6536 © 2025 IEEE. All rights reserved, including rights for text and data mining, and training of artificial intelligence and similar technologies. Personal use is permitted, but republication/redistribution requires IEEE permission.
See https://www.ieee.org/publications/rights/index.html for more information.

for predicting the VRU speed trajectory. The trajectory is approximated by a low-order polynomial, whose parameters are determined by the NN based on the historical speed profile input. Apart from neglecting the interaction with the vehicle, leaving the model to be unaware of the pedestrian's position may cause certain prediction errors, particularly near the crosswalk edge where pedestrians could abruptly change their decisions and speed trajectory trends. A nonlinear MPC (NMPC)-based safe speed problem is formulated in [13], which attempts to unify intelligent speed adaptation (ISA) and emergency braking assist (EBA) functionalities. If it is predicted that the pedestrian is on a collision course with the vehicle, the NMPC law activates a vehicle position constraint to avoid the collision. However, prediction of the collision course and related uncertainties are not dealt with.

To account for vehicle-pedestrian interaction, the pedestrian crossing decision is predicted in [5] by feeding a support vector machine model with the expected time taken by the vehicle to reach the pedestrian at the current speed (a gap acceptance model). The accuracy of the approach can be affected by discrepancies in forthcoming vehicle speed from the assumed current one. Furthermore, interaction-aware models used in literature are mostly executed independently of the MPC optimization algorithm (i.e., sequentially to gain computational efficiency). Such an approach is used for instance in [14] for AV control in interaction with other vehicles at multilane turn intersections, where an LSTM-type NN provides predictions to MPC. Another example is [15], where a vehicle path planning algorithm is activated to avoid collision upon getting short-term predictions of upcoming pedestrian action in safety-critical situations. To fully account for the vehicle-pedestrian interaction, related prediction models should be integrated within MPC optimization, as it is suggested in [16] for AV lane change tasks in interaction with surrounding vehicles. A prediction model anticipating future trajectories of other agents, as presented in [17], encodes an interaction aspect by conditioning predictions with respect to an ego-vehicle future motion plan and setting the basis for its optimization. In [18], the pedestrian velocity is modeled as an additional state variable through a simplified nonlinear static function of time-to-collision (TTC) between vehicle and pedestrian, so that the vehicle can account for its influence on the pedestrian (via TTC) while planning trajectory through the MPC law. In general, the interactive MPC optimization problem is scarcely tackled in literature, especially in the context of AV-pedestrian interactions, and it represents the main subject of this article.

Alternative approaches to account for interactions and related uncertainties in a systematic manner are reinforcement learning (RL)-based and partially observable Markov decision process (POMDP) methods. For instance, a model-free, deep RL (DRL) approach is deployed in [19] as a type of safety manifold providing AV-safe cruising speed. In general, the RL methods could be fragile, as they are typically sample inefficient and require an excessive amount of data to converge [20]. This drawback is mitigated in [19] by decoupling the high-level DRL-based safe speed control from a low-level autonomous driving system. Thornton et al. [21] formulated the problem of autonomous driving near

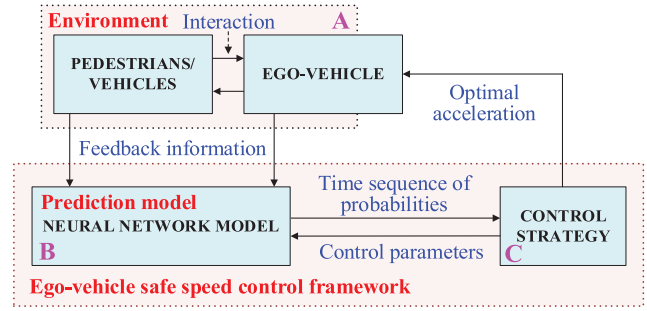

Fig. 1. Conceptual block diagram of overall AV safe speed control system.

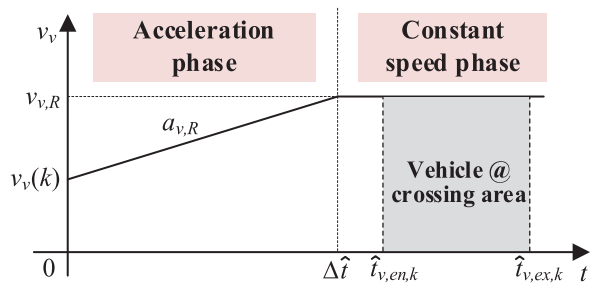

Fig. 2. Illustration of the definition of vehicle control trajectory parameters: reference acceleration $a_{v,R}$ and reference speed $v_{v,R}$.

pedestrians as POMDP, and solve it offline by using dynamic programming (DP) algorithm to obtain a related control policy. The POMDP reward function includes human values such as safety, legality, and mobility, which are transferred from the qualitative description and engineering specifications to mathematical expressions [22]. Similarly, POMDP is applied in [23] for AV control in an unstructured environment with pedestrians. The POMDP optimization problem is solved online therein to tackle high problem dimensionality. An alternative is to learn AV control from expert demonstrations, e.g., from human drivers, in an end-to-end learning manner (from sensor measurements directly to control actions) [24]. The offline execution is the main advantage of imitation learning when compared to RL, as the latter learns by trial-and-error and can, thus, be critical from the safety perspective. The main drawbacks of imitation learning are attributed to an excessive amount of training data needed to cover a wide range of situations that could be encountered in real-world driving, and a bias of the obtained control policy toward the training data used. Another example of imitation learning is given in [25], where human drivers approaching a crosswalk with pedestrians are modeled by using a stochastic Gaussian mixture model, for the purpose of setting the Baseline for different AV control strategies.

To fill the research gaps described above, this article proposes a model-based interaction- and uncertainty-aware AV safe speed control framework, which is conceptually described in Fig. 1. It consists of an NN-based prediction model of pedestrian crossing behavior (Block B) and a grid-based SMPC algorithm aimed to optimally control the vehicle while approaching the crosswalk (Block C). The innovative

interaction-aware aspect is reflected in the control strategy accounting for predicted pedestrian reaction on the hypothetical ego vehicle's actions (see connections of Blocks B and C). To simplify the learning problem, instead of predicting the whole pedestrian trajectories, the proposed NN model focuses solely on pedestrian-crosswalk entry and exit time predictions, as the relevant quantities from the perspective of approaching vehicle (similarly, Völz et al. [2] narrow prediction to pedestrian time-to-cross and distance-to-cross values). To capture the inherent uncertainty of pedestrian behavior, the conditional probability distributions of entry and exit time over the prediction horizon are formulated. These distributions can be considered as an exact representation of pedestrian crossing uncertainty, as they can be explicitly learned from data via supervised learning. In literature, pedestrian crossing uncertainty is often considered by propagating process noise through prediction model [5], [10], [11], and related future pedestrian positions (to be avoided by vehicle) are conservatively approximated with rectangles [5] or ellipses [12]. Uncertainties can also be accounted for by generating multiple potential pedestrian trajectories [9], or via probability distributions over system states (belief) as a part of the POMDP approach [23]. The proposed scenario-based SMPC strategy iteratively examines different vehicle speed trajectories along with NN model pedestrian predictions in an integrated manner (within one sampling time step), in order to find the one that minimizes the expected vehicle traveling time while keeping the probability of collision with pedestrian low. To reduce the numerical complexity, the vehicle speed trajectory is described by only two control parameters: the target acceleration and the target speed (see Fig. 2); as proposed in [26] for AV control while driving toward traffic lights, and where it is shown that this simplification has a minor effect on control performance when compared to use of free sequence of accelerations. As these control parameters also serve as NN model inputs (see interaction between Blocks B and C in Fig. 1), the NN model architecture is also simplified in this way. To further improve numerical efficiency, at the cost of somewhat higher implementation complexity, the vehicle prediction model is developed in a static form based on the piecewise-uniform acceleration assumption. The model determines the vehicle traveling time for different control scenarios. The proposed control framework is verified by means of Monte Carlo simulations for single-vehicle/single-pedestrian interactions, where the pedestrian is simulated according to a previously developed game theory-based model [27], [28] (Block A in Fig. 1).

The main contributions of this article include: 1) a fully interaction-aware safe speed SMPC framework integrating pedestrian prediction model and control optimization; 2) capturing pedestrian crossing uncertainties via probability distributions of pedestrian entry and exit time; and 3) a numerically efficient scenario-based SMPC strategy relying on a simplified vehicle speed trajectory-related static prediction model and a NN-based pedestrian behavior prediction model. This article extends upon the previous authors' conference publication [29] in terms of considering more realistic time-varying pedestrian behavior, practical and numerically efficient static vehicle prediction model, and more comprehensive test scenarios. The proposed stochastic control framework and related algorithms can find wider applications that are of interest to the control community, including interaction of AV with other road users (e.g., other vehicles during the lane change maneuver), robotics control in uncertain environments, and unmanned aerial vehicle control.

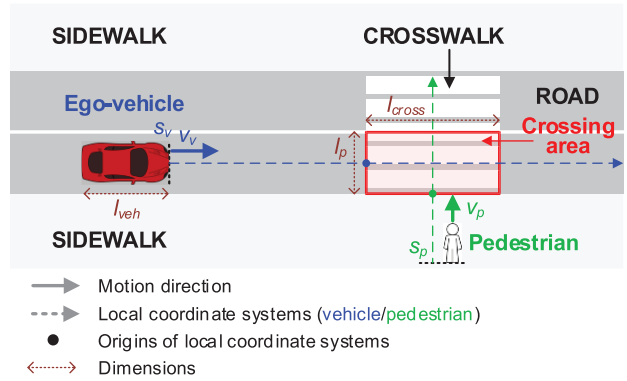

Fig. 3. Illustration of single-vehicle/single-pedestrian simulation framework.

The remaining part of this article is organized as follows. Section II briefly describes the game theory-based pedestrian crossing behavior simulation model. Section III presents the NN prediction model of pedestrian crossing behavior. Sections IV and V elaborate on SMPC-based safe speed control strategy. The large-scale simulation verification results are presented in Section VI. Concluding remarks are given in Section VII. Notation section explains the most common variable symbols and indices.

II. Game Theory Pedestrian Model

This section presents the simulation framework and overviews the game theory-based pedestrian crossing behavior model (Block A in Fig. 1) [27], [28].

A. Simulation Framework

It is assumed that the vehicle follows its road lane, while the pedestrian approaches the crosswalk perpendicularly to the road (see Fig. 3). The motion of both agents is simulated according to the following discrete-time state space model:

$$\begin{bmatrix} s_x(k+1) \\ v_x(k+1) \end{bmatrix} = \begin{bmatrix} 1 & \Delta T \\ 0 & 1 \end{bmatrix} \begin{bmatrix} s_x(k) \\ v_x(k) \end{bmatrix} + \begin{bmatrix} 0.5\Delta T^2 \\ \Delta T \end{bmatrix} a_x(k) \tag{1a}$$

which is obtained by zero-order-hold discretization of its continuous-time counterpart

$$\begin{bmatrix} \dot{s}_x(t) \\ \dot{v}_x(t) \end{bmatrix} = \begin{bmatrix} 0 & 1 \\ 0 & 0 \end{bmatrix} \begin{bmatrix} s_x(t) \\ v_x(t) \end{bmatrix} + \begin{bmatrix} 0 \\ 1 \end{bmatrix} a_x(t), \quad x \in \{p, v\} \tag{1b}$$

and where s_x, v_x, and a_x are agents' position, speed, and acceleration; the subscript $x \in \{p, v\}$ stands for pedestrian or vehicle, k is the discrete step, and $\Delta T = 0.1$ s is the corresponding time step (see Notation section for details on composing variable symbols). The agents' positions s_x are expressed in their local coordinate systems having the origins

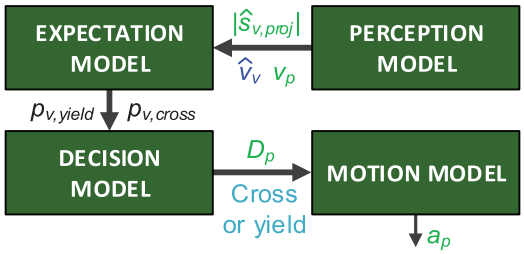

Fig. 4. Principal block diagram of a pedestrian crossing behavior model.

at the crosswalk leading edges (see Fig. 3). Accordingly, the agents' statuses are defined as

$$S_x(k) = \begin{cases} -2, & \text{if } s_x(k) \ll 0 \text{ m} \\ -1, & \text{else if } s_x(k) \leq 0 \text{ m} \\ 0, & \text{else if } 0 < s_x(k) < l_x \\ 1, & \text{else if } s_x(k) \geq l_x, \end{cases} \quad x \in \{p, v\} \tag{2}$$

with the following meaning: not appeared yet (−2), ahead of crossing area (−1), on crossing area (0), and behind crossing area (1), where l_x denotes the coordinate of the agents when traversing the crossing area trailing edge, which are given by $l_v = l_{\text{cross}} + l_{\text{veh}} = 4 + 5 = 9$ m and $l_p = 2.5$ m (for neglected pedestrian length, Fig. 3).

B. Pedestrian Model

The pedestrian model is adopted from [27], and extended as presented in [28] to 1) introduce variability/uncertainty in the pedestrian crossing behavior and 2) account for the pedestrian to be at any position s_p (rather than only on the crosswalk edge, $s_p = 0$). The model is organized around the following distinct submodels (see Fig. 4, [27], [28]): 1) perception; 2) expectation; 3) decision; and 4) motion submodels. The *perception model* emulates pedestrian sensing in terms of estimating/perceiving the vehicle's position s_v and speed v_v. The *expectation model* provides the probability of the vehicle crossing decision $p_{v,\text{cross}}$. The model is based on a binary logistic regression, whose inputs are the actual pedestrian speed v_p, the perceived vehicle speed $\hat{v}_v$, and the projected vehicle position $\hat{s}_{v,\text{proj}}$ at the instant at which the pedestrian is expected to reach the crosswalk (see the expression (5) and Fig. 4). The probability of opposite (yielding) decision is then simply calculated as $p_{v,\text{yield}} = 1 - p_{v,\text{cross}}$. The *decision model* provides the pedestrian decision D_p, where $D_p = 0$ for yield, and $D_p = 1$ for cross decision. The model relies on quantifying the goodness of each decision through so-called prospects derived from the cumulative prospect theory [30]. These prospects (one per each of two decisions) mainly depend on the probabilities provided by the expectation model, and the decision with a larger prospect is adopted as the current decision $D_p(k)$.

The *motion model* is based on (1a), where the pedestrian acceleration $a_p(k)$ is determined in dependence on the decision $D_p(k)$ as

$$a_p(k) = \begin{cases} -\dfrac{v_p^2(k)}{2\left|s_p(k)\right|}, & \text{if } D_p = 0 \\ a_{p,\max}\operatorname{sgn}\left(v_{p,\text{dev}}\right), & \text{if } D_p = 1 \end{cases} \tag{3a}$$

where $a_{p,\max}$ is the maximum acceleration set here to an arbitrary value of 2 m/s^2, $v_{p,\text{dev}}$ is the deviation of the current pedestrian speed $v_p(k)$ from the one prescribed at the beginning of the interaction simulation $v_{p,0}$

$$v_{p,\text{dev}} = \begin{cases} 0, & \text{if } \left|v_{p,0} - v_p(k)\right| < 0.1 \\ v_{p,0} - v_p(k), & \text{otherwise} \end{cases} \tag{3b}$$

where a small dead-zone is introduced to avoid a chattering effect for $v_{p,0} - v_p(k) \approx 0$, and where $\operatorname{sgn}(\cdot)$ is the signum function defined as

$$\operatorname{sgn}(x) = \begin{cases} -1, & \text{if } x < 0 \\ 0, & \text{if } x = 0 \\ 1, & \text{if } x > 0. \end{cases} \tag{3c}$$

Hence, for the yield decision ($D_p = 0$), the pedestrian is to uniformly decelerate to stop right at the edge of the crosswalk, while for the cross decision ($D_p = 1$), his/her acceleration is set to $\pm a_{p,\max}$ to accelerate/decelerate toward the initial pedestrian speed $v_{p,0}$.

To impose variability in the simulated pedestrian crossing behavior for testing the proposed control strategy under elevated uncertainty and risk conditions, a random perturbation of different pedestrian model inputs and parameters is introduced. The perception model perturbs the pedestrian-perceived feedback information by sampling from the normal distributions: $\hat{s}_v \sim \mathcal{N}(s_v, \varepsilon_{\max}|s_v|)$ and $\hat{v}_v = \max(0, \mathcal{N}(v_v, \varepsilon_{\max} v_v))$, where the first and second argument of $\mathcal{N}(\cdot,\cdot)$ represent the expectation and standard deviation, respectively, while $\varepsilon_{\max}$ is a tunable parameter denoting the perception error level. These perturbations propagate through the expectation and decision submodels, and indirectly introduce variability in pedestrian decisions D_p. Additional variability is introduced by multiplying the decision prospects with the following random variable (sampled from uniform probability distribution independently for each of the two prospects):

$$\varepsilon = 1 + \mathcal{U}(-1, 1)\varepsilon_{\max}. \tag{4}$$

Finally, the expectation and decision submodels' parameters are also perturbed, but only once per simulation, i.e., in the stage of its initialization. This is done by multiplying them with a random variable sampled separately for each parameter by using (4). In this way, different individual pedestrians are realized. The parameter $\varepsilon_{\max}$ is set to a relatively high value of 0.5 to test the proposed control strategy under more extreme conditions (less cautious pedestrians).

The adopted extended pedestrian model from [28] projects the vehicle distance to the estimated time instant $\Delta T_{p,\text{proj}}$ of pedestrian reaching the crosswalk edge [28]

$$\begin{aligned} \hat{s}_{v,\text{proj}}(k) &= \hat{s}_v(k) + \hat{v}_v(k)\,\Delta T_{p,\text{proj}}(k) \\ \Delta T_{p,\text{proj}}(k) &= \left|s_p(k)\right| / v_p(k). \end{aligned} \tag{5}$$

The projected vehicle distance $\hat{s}_{v,\text{proj}}$ is then used as the input of expectation and decision model input (see Fig. 4), which outputs the pedestrian decision D_p according to the following expression [28]:

$$D_p(k) = \begin{cases} D_{p,0} & \text{if } \hat{s}_v(k) \le 0 \wedge \hat{s}_{v,\text{proj}}(k) \le 0 \text{ m} \\ 0, & \text{else if } \hat{s}_v(k) < l_v \wedge \hat{s}_{v,\text{proj}}(k) > 0 \text{ m} \\ 1, & \text{else if } \hat{s}_v(k) \ge l_v \vee s_p > 0 \text{ m} \end{cases} \tag{6}$$

where $D_{p,0}$ is the decision corresponding to the nominal case of both actual and projected vehicle being in front of the crosswalk, and made by calculating and comparing the prospects [27].

The above pedestrian model is slightly modified in [31] by including additional inputs such as vehicle and pedestrian accelerations, and it is reparameterized and validated with respect to the experimental in D dataset recorded in the city of Aachen, Germany [32]. It is demonstrated in [31] that the model results in solid accuracy against the experimental data, thus confirming its ability to capture the actual pedestrian crossing behaviors.

III. NN Pedestrian Prediction Model

This section overviews the NN model aimed at predicting the pedestrian crossing behavior on a receding horizon (Block B in Fig. 1, [33]).

A. Problem Definition

From the perspective of vehicle control, two quantities are of interest to be predicted: the pedestrian entry ($t_{p,\text{en}}$) and exit time ($t_{p,\text{ex}}$) from the crossing area, as they define the occupancy of the conflicting crossing area (see Fig. 3). In order to capture the inherent variability of pedestrian behavior, a supervised learning task is formulated, which gives the entry/exit time conditional probability distributions on the prediction time horizon $\tilde{\mathbf{t}} = [\tilde{t}_j = j\Delta T]$, $j = 1, 2, \ldots, N$, where $\tilde{t}_j$ is defined as the relative time with respect to the current (kth) time step (i.e., $\tilde{t}_0 = 0$ s). Thus, the pedestrian entry time conditional probability distribution is defined as

$$\hat{p}_{\text{en},k,j} = P(t_{p,\text{en},k} = \tilde{t}_j | \mathbf{Z}_k) \tag{7a}$$

where $\hat{p}_{\text{en},k,j}$ is the probability that the pedestrian entry time $t_{p,\text{en},k}$ will be realized at the jth step time $\tilde{t}_j$ of prediction horizon, and it is determined from the input feature vector $\mathbf{Z}_k$ that includes the current vehicle and pedestrian states ($s_{v,k}$, $v_{v,k}$, $s_{p,k}$, and $v_{p,k}$) and the vehicle control parameters ($v_{v,R,k}$ and $a_{v,R,k}$, defined in Fig. 2). Similarly, the pedestrian exit time conditional probability distribution is defined as

$$\hat{p}_{\text{ex},k,j} = P\left(t_{p,\text{ex},k} = \tilde{t}_j | \left[\mathbf{Z}_k \hat{t}_{p,\text{en},k}\right]\right) \tag{7b}$$

where the input feature vector is extended with a presumed entry time value $\hat{t}_{p,\text{en},k}$, which is selected by the control strategy to obtain the joint probability of a certain combination of entry and exit time values (see Sections IV and V for more details). The probabilities from (7) can be written in a vector form as $\hat{p}_{\text{en},k} = [\hat{p}_{\text{en},k,j}]$ and $\hat{p}_{\text{ex},k} = [\hat{p}_{\text{ex},k,j}]$, $j \in [1, 2, \ldots, N]$. The prediction horizon length of $N = 100$ steps is used here,

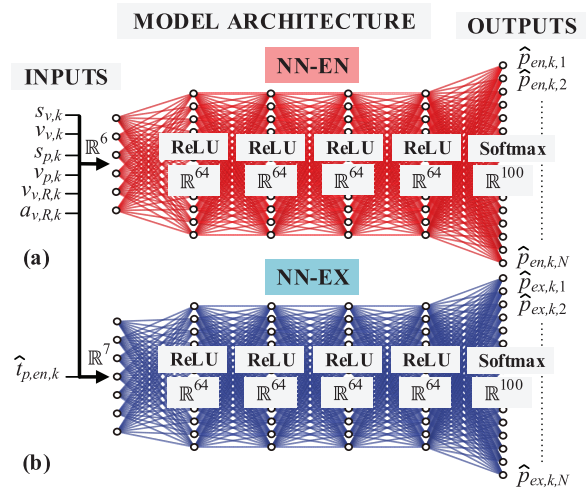

Fig. 5. Architecture of NN models used for prediction of pedestrian (a) entry time and (b) exit time.

which corresponds to the prediction horizon $\tilde{t}_N = 10$ s for the sampling time $\Delta T = 0.1$ s.

It should be noted that the proposed prediction model structure is flexible in terms of representing a probability distribution of an arbitrary complexity (see Fig. 5). Thus, it should be capable of capturing a wide range of pedestrian behaviors, if having appropriate training data, so that the corresponding control strategy is not limited to the considered game theory pedestrian model.

B. Prediction Model

Two NN models have been built up to model the probability distributions (7) (see Fig. 5). The supervised learning problem can be regarded as a classification task [34], because the prediction horizon discrete time steps $\tilde{\mathbf{t}}$ can be interpreted as classes to which the model assigns the probabilities. Thus, a negative log-likelihood (NLL) loss function, typically used in classification tasks, is employed, and it is defined as (for the NN-EN model; and also the NN-EX model, where the subscript en is replaced with ex)

$$\text{NLL} = \frac{1}{M} \sum_{i \in S} \sum_{k \in K_i} \left(-\sum_{j=1}^{N} Y^i_{\text{en},k,j} \log\left(\hat{p}^i_{\text{en},k,j}\right) \right) \tag{8}$$

where index i refers to ith simulation/interaction from the considered dataset S (e.g., the training dataset), k denotes the time step of ith simulation and K_i is the dataset containing selected simulation steps from ith simulation, and $\mathbf{Y}^i_{\text{en},k} = [Y^i_{\text{en},k,j}]$ is the one-hot vector having the prediction horizon length N and encoding the information on actual pedestrian entry time $t^i_{p,\text{en},k}$ as

$$Y^i_{\text{en},k,j} = \begin{cases} 1, & \text{if } \tilde{t}_j = t^i_{p,\text{en},k} \\ 0, & \text{otherwise.} \end{cases}$$

Fig. 5 shows the selected deep feedforward NN models (see Section III-C and [33] for more details on NN architecture selection), with the ReLU activation function contained in the hidden layers, and softmax included in the output layer.

The latter is used to ensure that the model outputs are valid probability distributions, satisfying the following conditions:

$$\sum_{j=1}^{N} \hat{p}_{\text{en(ex)},k,j} = 1, \quad \hat{p}_{\text{en(ex)},k,j} \in [0,1] \quad \forall\ k, j.$$

C. Data Generation and NN Training

As the pedestrian behavior prediction represents a key part of the overall control system, meaning that poor characterization or coverage may lead to poor performance or lack of robustness in the overall control system, the following is conducted to ensure a sufficiently large, representative, and well-balanced simulation dataset is utilized for the control system development. In the particular study, the data needed for pedestrian prediction model development have been generated by conducting numerous simulations of the game theory pedestrian model (see Section II) for the vehicle driven in an open-loop manner. Each simulation is set to start with the vehicle approaching the crosswalk from the fixed initial position (set to $s_{v,0} = -100$ m). The vehicle speed is kept at the initial value $v_{v,0}$ until the selected instant of pedestrian appearance $T_{p,0}$ when the vehicle starts to follow the saturated linear speed trajectory defined by the control parameters $a_{v,R}$ and $v_{v,R}$ (see illustration in Fig. 2). The initial conditions are generated randomly for each simulation by sampling from the following probability distributions: $v_{v,0}$ [m/s] $\sim \mathcal{N}(7.5, 2^2)$, $v_{v,R}$ [m/s] $\sim \mathcal{N}(7.5, 2^2)$, $T_{p,0}$ [s] $\sim \mathcal{U}(0, \text{TTA}_v)$, $s_{p,0}$ [m] $\sim \mathcal{N}(-4, 0.8^2)$, $v_{p,0}$ [m/s] $\sim \mathcal{N}(1.38, 0.27^2)$, where the parameters for $v_{v,0}$, $v_{v,R}$, and $v_{p,0}$ are adopted from [27], while those for $s_{p,0}$ are set arbitrarily, and where $\text{TTA}_v = |s_{v,0}|/v_{v,0}$ is predicted vehicle time-to-arrival to the crosswalk. The target acceleration $a_{v,R}$ is generated as ($a_{v,\max} = 2$ m/s^2)

$$a_{v,R} = r \cdot a_{v,\max} \cdot \text{sgn}\left(v_{v,R} - v_{v,0}\right); \quad r \sim \mathcal{U}(0,1).$$

In total, 10000 vehicle-pedestrian interaction simulations were run. Two datasets were randomly created from the simulation data samples, $(\mathbf{Z}_k^i, \mathbf{Y}_{\text{en},k}^i)$ and $([\mathbf{Z}_k^i t_{p,\text{en},k}^i], \mathbf{Y}_{\text{ex},k}^i)$, and divided into training, validation, and testing subsets, with the shares of 60%, 20%, and 20% of the total data, respectively.

The model inputs $\mathbf{Z}_k^i$ and $[\mathbf{Z}_k^i t_{p,\text{en},k}^i]$ were normalized into the interval $[-1, 1]$ for better numerical conditioning of NN training. The models were trained in a Python environment by using the Keras module [35] with TensorFlow [36] as backend, and ADAM optimization algorithm [37]. The optimal NN model architecture shown in Fig. 5 was found by grid search over different NN configurations based on the criterion of the minimal NN-EN validation loss defined by (8) [33].

D. Results

The NLL loss function values for training, validation, and testing datasets are given in Table I for both NN models. The results show that the loss values are very similar for the three datasets, thus confirming that the models are properly trained, with no overfitting present.

Fig. 6 shows an example of prediction model responses. Two distinct probability modes of the predicted entry time (red line) can be observed in the plot. They relate to two characteristic outcomes, i.e., when the pedestrian passes the crosswalk prior to or after the vehicle. The time interval of the vehicle passing the crosswalk (shaded region in Fig. 6) is projected/estimated on the prediction horizon from the current vehicle state (s_v, v_v) and the vehicle control parameters $(v_{v,R}, a_{v,R})$ based on the expression (20) given below. Fig. 6 also includes two examples of NN-EX model predictions depending on the presumed entry time input $\hat{t}_{p,\text{en},k}$. The exit time probability distributions are naturally delayed with respect to entry time, where the width of distribution depends on the vehicle and pedestrian states.

The models are validated against the ground truth simulation results based on different probability and entry/exit

TABLE I
NLL LOSS VALUES FOR ENTRY AND EXIT TIME NN MODELS AND DIFFERENT DATASETS

	LOSS VALUE		
	Train	**Validation**	**Test**
NN-EN	1.924	1.997	2.049
NN-EX	1.862	1.863	1.877

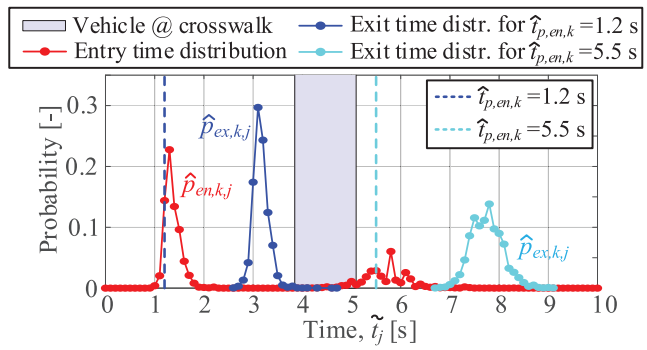

Fig. 6. Example of prediction of pedestrian entry and exit time probability distributions obtained for $s_{v,k} = -25$ m, $v_{v,k} = 4.6$ m/s, $s_{p,k} = -1.8$ m, $v_{p,k} = 1.5$ m/s, $a_{v,R,k} = 1.2$ m/s^2, and $v_{v,R,k} = 7.2$ m/s.

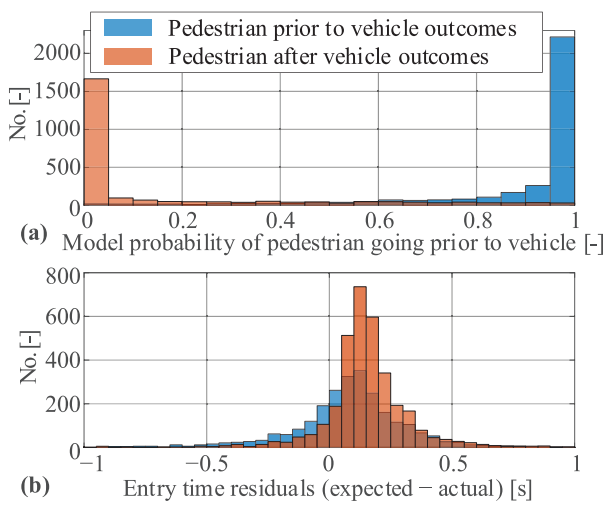

Fig. 7. Aggregate probabilities of pedestrian going prior to vehicle derived from (a) NN-EN model outputs against actual simulation outcomes, and (b) model entry time residuals.

time metrics [33]. First, the NN-EN model output probability distribution is divided into two modes illustrated in Fig. 6: pedestrian surpasses 1) prior to the vehicle and 2) after the vehicle. Then, the aggregate probability of the pedestrian going prior to the vehicle is calculated by summing up all the first mode probabilities. The results shown in Fig. 7(a) indicate that a great majority of high probabilities correspond to the target outcome of pedestrian passing prior to the vehicle; and similarly, a great majority of low probabilities relate to the opposite outcome. Apart from the aggregate probabilities, the entry time model residuals are analyzed. First, the entry time expectations of the first and second modes are calculated for each model prediction. Then, the actual entry time is subtracted from the closer entry time expectation to obtain the model residual. The results shown in Fig. 7(b) point out that the residual distributions fall within a narrow range close to zero (around ±0.5 s). More details on the model validation can be found in [33] and [38].

IV. Structure and Basic Functionalities of Safe Speed Control Strategy

A. Problem Definition

The aim of the proposed safe speed control strategy (Block C in Fig. 1) is to minimize the following two, generally conflicting objectives: 1) traveling time and 2) risk of collision with pedestrians. The traveling time $t_{v,\text{ex}}$ is defined as the time needed to exit/surpass the crosswalk (see Fig. 3)

$$t_{v,\text{ex}} = \arg_{t} \left(s_v(t) = l_v = l_{\text{veh}} + l_{\text{cross}}\right). \tag{9}$$

The collision is conservatively defined to occur ($C = 1$) if both agents are positioned within the crossing area at the same time

$$C = \begin{cases} 1, & \text{if } t_{p,\text{en}} \le t_{v,\text{en}} < t_{p,\text{ex}} \\ 0, & \text{otherwise.} \end{cases} \tag{10}$$

Note that based on (2) and (10) the condition $S_v(k) = 0 \bigwedge S_p(k) = 0$ should hold for $C = 1$ to be valid. The probability of collision as a measure of risk is then defined as

$$P_c = P(C = 1). \tag{11}$$

Note that the definition of conservativeness relates to the fact that both agents can be located within the crossing area, while still not resulting in collision due to the limited physical dimensions of pedestrian and vehicle. Thus, avoiding collision defined by (10) incorporates a certain safety margin which could be adjusted by "tuning" the crossing area width parameter l_p (see Fig. 3), including its enlargement to account for the situations when the vehicle is leaning to the road edge rather than being centered in the line.

B. High-Level Functionality

Depending on the presence of the pedestrian and his/her position relative to the crossing area, the control strategy is set to operate in one of the following three distinctive actions [see Fig. 8 and (2)].

Action 1: No relevant pedestrian is present ($S_p = -2 \bigvee S_p = 1$).

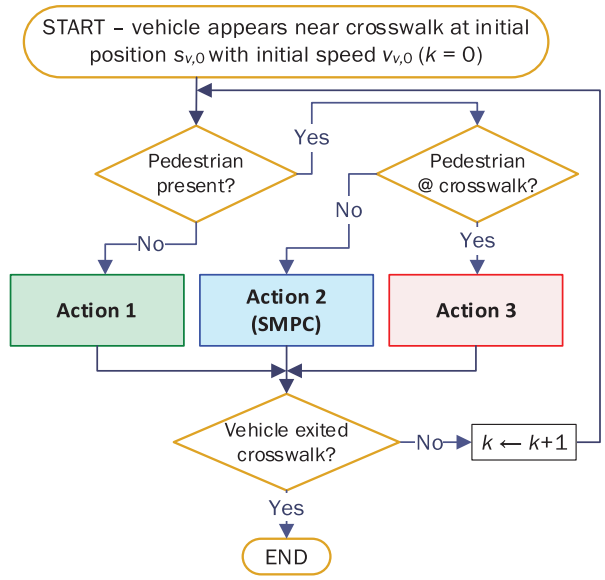

Fig. 8. High-level structure of vehicle safe speed control.

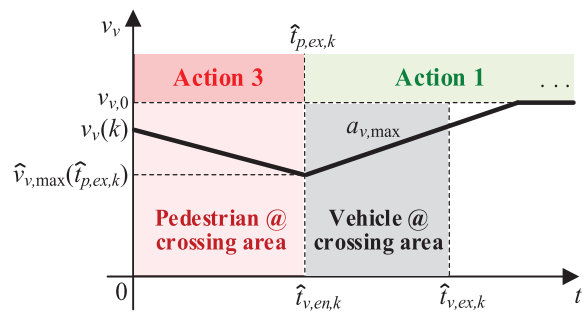

Fig. 9. Illustration of Action 3 followed by Action 1.

Action 2: There is a pedestrian approaching the crosswalk ($S_p = -1$).

Action 3: The pedestrian steps on the crosswalk ($S_p = 0$).

The motivation for such organization of the control strategy is to separate relatively simple rule-based and low-uncertainty Actions 1 and 3 from the numerically more demanding, optimization-based, and high-uncertainty Action 2. To determine the vehicle acceleration $a_v(k)$, the control strategy should account for different scenarios, as well as pedestrian behavior and vehicle state prediction on the upcoming time horizon.

It should be mentioned that the proposed framework is not limited to the single-pedestrian scenario considered in this article. In the multipedestrian scenario, the focus could be on a single, most critical pedestrian selected from the group [39], e.g., the one detected to be the closest to the crosswalk edge. Another possibility is to retrain the NN prediction model of the same structure to provide the probability distributions of the entry time of the first pedestrian entering the crosswalk and the exit time of the last pedestrian leaving the crosswalk.

C. Action 1

From the perspective of the vehicle, its initial speed $v_{v,0}$ could be regarded as a preferable cruising speed while approaching the crosswalk. Prior to pedestrian appearance

($S_p = -2$), Action 1 simply keeps this speed by prescribing zero acceleration ($a_v(k) = 0$). After the pedestrian has surpassed the crosswalk ($S_p = 1$), while the vehicle is still approaching it ($S_v = -1$), the vehicle speed typically differs from the initial value $v_{v,0}$ due to the previous Action 2 control. In that case, and if $v_v(k) < v_{v0}$, Action 1 prescribes the maximum acceleration $a_{v,\max}$ (set to 2 m/s^2) to accelerate toward the initial speed v_{v0} (see Fig. 9); while the acceleration is set to zero, otherwise, to avoid deceleration

$$a_v(k) = \begin{cases} a_{v,\max}, & \text{if } v_v(k) < v_{v,0} \\ 0 \text{ m/s}^2, & \text{otherwise.} \end{cases} \tag{12}$$

D. Action 3

Action 3 is initiated when the pedestrian steps onto the crosswalk ($S_p = 0$) in terms of activating braking, if needed, to avoid collision defined by (10). To determine the required deceleration, the pedestrian exit time from the crossing area $\hat{t}_{p,\text{ex},k}$ (relative to the current sampling step k; see Notation section) is first predicted based on the constant-speed assumption (see Fig. 3)

$$\hat{t}_{p,\text{ex},k} = \frac{l_p - s_p(k)}{v_p(k)}. \tag{13}$$

Next, by assuming uniform deceleration and considering marginal collision avoidance, the maximum allowed vehicle speed at the pedestrian exit time $\hat{t}_{p,\text{ex},k}$ is given by the following expression (corresponding to the area s_v of the trapezoid with the height $\hat{t}_{p,\text{ex},k}$ in Fig. 9)

$$\hat{v}_{v,\max}\left(\hat{t}_{p,\text{ex},k}\right) = \frac{2\left|s_v(k)\right|}{\hat{t}_{p,\text{ex},k}} - v_v(k) \tag{14}$$

where a negative result would mean that stopping right at the edge of the crosswalk should take place before the time instant $\hat{t}_{p,\text{ex},k}$.

Finally, the related vehicle acceleration is determined as

$$a_v' = \begin{cases} \dfrac{-v_v^2(k)}{2\left|s_v(k)\right|}, & \text{if } \hat{v}_{v,\max} < 0 \\ -\dfrac{v_v(k) - \hat{v}_{v,\max}}{\hat{t}_{p,\text{ex},k}}, & \text{if } 0 \le \hat{v}_{v,\max} \le v_v(k) \\ 0 \text{ m/s}^2, & \text{otherwise} \end{cases} \tag{15a}$$

where the first condition relates to the aforementioned full-stop case, the second one corresponds to the case of vehicle decelerating but not stopping (see illustration in Fig. 9), while the third one relates to the case when deceleration is not needed to avoid collision (i.e., the vehicle keeps cruising). The final acceleration in kth step is saturated to the physically attainable range as

$$a_v(k) = \begin{cases} a_v', & \text{if } \left|a_v'\right| \le a_{v,\max} \\ a_{v,\max}\operatorname{sgn}\left(a_v'\right), & \text{otherwise.} \end{cases} \tag{15b}$$

V. Action 2—SMPC

A. Optimal Control Problem Formulation

Action 2 is based on the following optimization problem, which is solved on-line on the receding prediction horizon:

$$\min_{v_{v,R}, a_{v,R}} \; E\left(t_{v,\text{ex}}\right) \tag{16a}$$

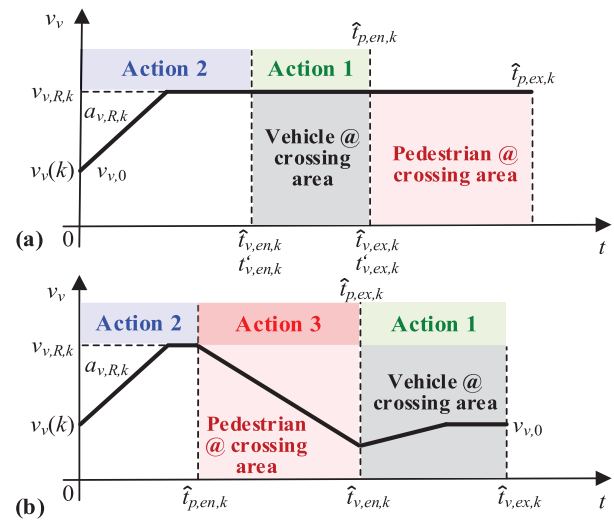

Fig. 10. Illustration of prediction horizon vehicle speed trajectory for scenarios of vehicle surpassing crosswalk prior to (a) and after pedestrian (b).

$$0 \le v_{v,R} \le v_{v,\max}, \quad -a_{v,\max} \le a_{v,R} \le a_{v,\max} \tag{16b}$$

$$P_c < \beta \tag{16c}$$

where $v_{v,R}$ and $a_{v,R}$ are the vehicle control parameters (see Fig. 2), (16a) is the vehicle traveling time expectation to be minimized, (16b) are the control parameter constraints (with $v_{v,\max} = 12$ m/s, and $a_{v,\max} = 2$ m/s^2), and (16c) is a chance constraint that limits the probability of collision P_c to a very low threshold β (set to $\beta = 0.001 = 0.1\%$). If the safety chance constraint (16c) cannot be satisfied for the current vehicle and pedestrian states, the minimization of the traveling time is replaced with the minimization of collision probability

$$\left\{v_{v,R}^*, a_{v,R,\text{abs}}^*\right\} = \begin{cases} \underset{v_{v,R}, a_{v,R}}{\operatorname{argmin}} \; E\left(t_{v,\text{ex}}\right), & \text{if } P_c < \beta, \; \exists v_{v,R}, a_{v,R,\text{abs}} \\ \underset{v_{v,R}, a_{v,R}}{\operatorname{argmin}} \; P_c, & \text{if } P_c \ge \beta \quad \forall v_{v,R}, a_{v,R,\text{abs}}. \end{cases} \tag{16d}$$

This is a stochastic optimization problem since it involves the cost function expectation operator E and the chance constraint (16c).

To solve the optimal control problem (16), the vehicle exit time $t_{v,\text{ex}}$ and the collision probability P_c should be calculated for different values of nominated control parameters $v_{v,R}$ and $a_{v,R}$. Instead of using the vehicle dynamics model (1a), a static/algebraic vehicle model is derived (see Appendix) based on the piecewise-uniform form of the speed profile defined in Fig. 2. This improves the overall numerical efficiency since the static model is computationally inexpensive. If the dynamic model (1a) were used, it would need to be evaluated on a prediction horizon of sufficiently large length in each sampling step (to encompass the vehicle surpass of the crosswalk and calculate the traveling time, see [26], [29], [40]), while the static model performs one-shot calculations.

Apart from core Action 2, activation of Actions 3 and 1 on the prediction horizon should also be accounted for when calculating the quantities of interest. To this end, two basic

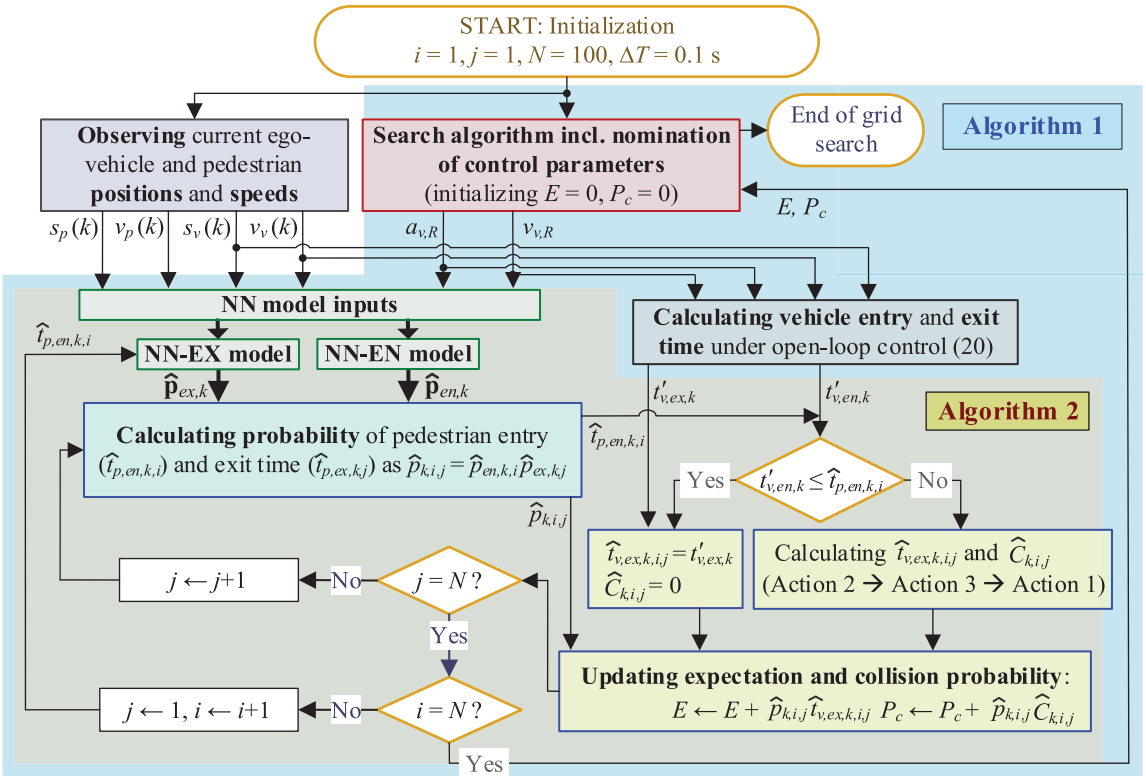

Fig. 11. Block diagram of Action 2-related control on the prediction horizon (details of Algorithms 1 and 2).

cases could occur while the vehicle approaches the crosswalk: 1) the vehicle surpasses the crosswalk prior to the pedestrian, and no intervention of Action 3 is needed to avoid collision [see Fig. 10(a)]; and 2) the pedestrian enters the crosswalk prior to the vehicle, and the vehicle activates Action 3 to decelerate and avoid collision [see Fig. 10(b)]. After the vehicle enters the crosswalk or after the pedestrian exits the crosswalk, Action 1 is activated as there is no active interaction with the pedestrian anymore.

B. Solving Optimal Control Problem

In typical SMPC applications, the variables introducing uncertainty are referred to as disturbances, and their probability distributions are assumed not to depend on control variables, which allows for casting the optimization problem into a standard LP/QP form solvable by available solvers [41]. Such an approach cannot be applied to the optimal control problem (16) in a straightforward manner, because of the inherent dependence of the chance constraint (16c) on the control parameters $v_{v,R}$ and $a_{v,R}$ (recall that the control parameters are used as the inputs of NN prediction models, Fig. 5). To overcome this issue and provide the global optimal solution, a grid search over all combinations of discretized control parameters is performed, i.e., a grid-based approach is applied in a similar way as in [42].

The control parameter grid values considered are $v_{v,R}$ [m/s] $\in \{0, 1, 2, \ldots, 12\}$ and $a_{v,R,\text{abs}}$ [m/s^2] $\in \{0, 0.2, 0.4, \ldots, 2\}$ (with $N_{v_{v,R}} = 13$ and $N_{a_{v,R,\text{abs}}} = 11$ elements). The applied control variable discretization has been found to have a negligible impact on the accuracy of the solution by comparing the solution with that obtained by the global search optimization algorithm Dividing Rectangles (DIRECT, [43]; run extensively, i.e., with a high maximum number of evaluations to end in the globally optimal solution).

Algorithm 1 Search for Optimal Control Parameters

- Initialize $\hat{t}_{v,ex,min}$ to a very large value.

for each $v_{v,R}$ **from** $\{0, 1, 2, \ldots, 12\}$ m/s
  for each $a_{v,R,abs}$ **from** $\{0, 0.2, 0.4, \ldots, 2\}$ m/s^2
    Execute **Algorithm 2** to get $E(t_{v,ex})$ and P_c
    if $\left(E(t_{v,ex}) < \hat{t}_{v,ex,\min}\right) \wedge (P_c < \beta)$
      $v^*_{v,R} = v_{v,R}$, $a^*_{v,R,abs} = a_{v,R,abs}$
      $\hat{t}_{v,ex,\min} = E(t_{v,ex})$
    end if
  end for
end for

- Calculate the final acceleration a_v to be applied by (17)

Solving the optimization problem (16) (see Algorithm 1 and the block diagram in Fig. 11) yields the optimal absolute reference acceleration $a^*_{v,R,\text{abs}}(k)$ and the target speed $v^*_{v,R}(k)$, which are used to extract the vehicle acceleration $a_v(k)$ applied in the actual (kth) sampling step

$$a_v(k) = a^*_{v,R,\text{abs}}(k)\,\text{sgn}\left(v^*_{v,R}(k) - v_v(k)\right). \tag{17}$$

The procedure is repeated in the next sampling steps.

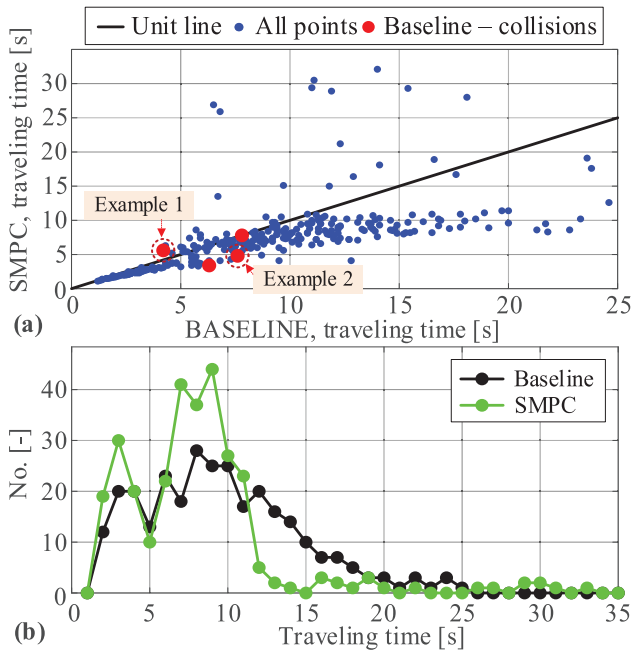

Fig. 12. Comparison of vehicle traveling time values (a) and respective histograms (b) obtained by applying SMPC and Baseline control strategies for 300 vehicle-pedestrian interactions.

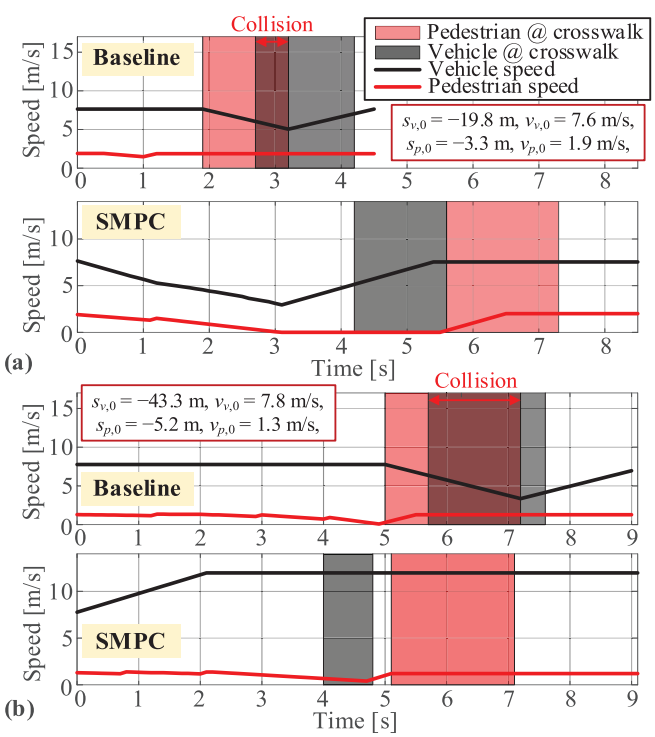

Fig. 13. Vehicle and pedestrian speed trajectories obtained by applying Baseline control and SMPC in collision-outcome interactions designated in Fig. 12 as (a) Example 1 and (b) Example 2.

C. Calculating Vehicle Traveling Time Expectation and Probability of Collision

From the standpoint of vehicle control, the pedestrian crossing behavior is characterized by considering all possible combinations of the pedestrian entry ($\hat{t}_{p,\mathrm{en},k}$) and exit

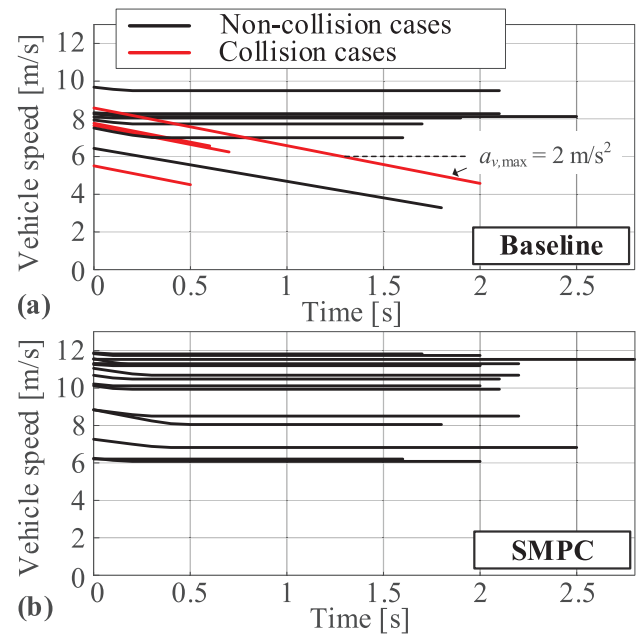

Fig. 14. Vehicle speed trajectories under Action 3 for (a) Baseline control and (b) SMPC.

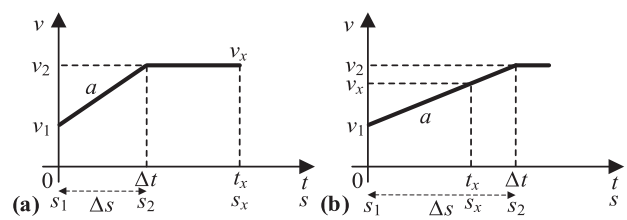

Fig. 15. Illustration of characteristic speed trajectories for piecewise-uniform acceleration motion for case of reaching (a) target speed v2 at considered time instant tx and not reaching it (b).

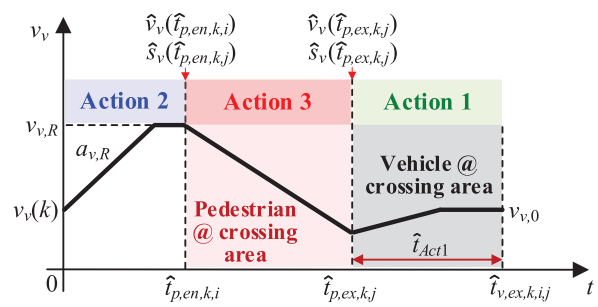

Fig. 16. Illustration of vehicle speed trajectory on prediction horizon for the case of a pedestrian entering crosswalk prior to vehicle.

time ($\hat{t}_{p,\mathrm{ex},k}$) on the prediction horizon $\tilde{\mathbf{t}} = [\tilde{t}_j = j\Delta T]$, $j \in \{1, 2, \ldots, N\}$. The joint probability of an entry and exit time combination, i.e., $\hat{t}_{p,\mathrm{en},k,i} = i\Delta T$ and $\hat{t}_{p,\mathrm{ex},k,j} = j\Delta T$, with $j > i$, is calculated as

$$\hat{p}_{k,i,j} = \hat{p}_{\mathrm{en},k,i} \cdot \hat{p}_{\mathrm{ex},k,j} \tag{18}$$

where the probability $\hat{p}_{\mathrm{en},k,i}$ of pedestrian entry time to take on the value $\hat{t}_{p,\mathrm{en},k,i}$ is provided by the NN-EN prediction model depending on the input feature vector $\mathbf{Z}_k$ [see Fig. 5(a)], while

Algorithm 2 Calculating $E(t_{v,\mathrm{ex}})$ and P_c for a Given Set of Control Parameters $v_{v,R}$ and $a_{v,R}$

- Calculate vehicle entry time ($t'_{v,en,k}$) according to (20), and exit time ($t'_{v,ex,k}$) according to (20) with substitution of $|s_v(k)|$ with $|s_v(k)| + l_v$.
- Initialize $E(t_{v,ex}) = 0$ (denoted as E) and $P_c = 0$.

for each $\hat{t}_{p,en,k,i}$ **from** $\tilde{\mathbf{t}} = [\tilde{t}_i = i\Delta T], i = 1,2,\ldots,N$
  Obtain $\hat{p}_{en,k,i}$ from NN-EN model
  for each $\hat{t}_{p,ex,k,j}$ **from** $\tilde{\mathbf{t}}$ for which $\hat{t}_{p,ex,k,j} > \hat{t}_{p,en,k,i}$
    Obtain $\hat{p}_{ex,k,j}$ from NN-EX model
    Calculate $\hat{p}_{k,i,j} = \hat{p}_{en,k,i} \cdot \hat{p}_{ex,k,j}$ using (18)
    if $t'_{v,en,k} \le \hat{t}_{p,en,k,i}$
      $\hat{C}_{k,i,j} = 0$, $\hat{t}_{v,ex,k,i,j} = t'_{v,ex,k}$ using (21)
    else if $t'_{v,en,k} > \hat{t}_{p,en,k,i}$
      Calculate $\hat{C}_{k,i,j}$ and $\hat{t}_{v,ex,k,i,j}$ using (23) and (27), respectively
    end if
    Update P_c and E according to (19) as:
    $E \leftarrow E + \hat{p}_{k,i,j}\hat{t}_{v,ex,k,i,j}, P_c \leftarrow P_c + \hat{p}_{k,i,j}\hat{C}_{k,i,j}$
  end for
end for

the probability $\hat{p}_{\mathrm{ex},k,j}$ of pedestrian exit time to assume the value $\hat{t}_{p,\mathrm{ex},k,j}$ is outputted by the NN-EX model fed by the vector $\mathbf{Z}_k$ and the considered entry time $\hat{t}_{p,\mathrm{en},k,i}$ [see Fig. 5(b)].

The vehicle traveling time expectation (16a) and the probability of collision (16c) can be calculated as (see Algorithm 2 and also the block diagram shown in Fig. 11)

$$E\left(t_{v,\mathrm{ex}}\right) = \sum_{i=1}^{N}\sum_{j=i+1}^{N} \hat{p}_{k,i,j}\hat{t}_{v,\mathrm{ex},k,i,j} \tag{19a}$$

$$P_c = \sum_{i=1}^{N}\sum_{j=i+1}^{N} \hat{p}_{k,i,j}\hat{C}_{k,i,j} \tag{19b}$$

where $\hat{t}_{v,\mathrm{ex},k,i,j}$ is the predicted vehicle traveling time for the given values of pedestrian entry and exit times on the prediction horizon $\hat{t}_{p,\mathrm{en},k,i} = i\Delta T$ and $\hat{t}_{p,\mathrm{ex},k,j} = j\Delta T$, respectively, $\hat{p}_{k,i,j}$ is the corresponding joint probability defined by (18), and $\hat{C}_{k,i,j}$ is the collision flag based on (10). Thus, the vehicle traveling time prediction $\hat{t}_{v,\mathrm{ex},k,i,j}$ and the collision flag $\hat{C}_{k,i,j}$ are functions of the current vehicle position $s_v(k)$ and speed $v_v(k)$, the control parameters $v_{v,R}$ and $a_{v,R}$, and the pedestrian entry and exit time predictions $\hat{t}_{p,\mathrm{en},k,i}$ and $\hat{t}_{p,\mathrm{ex},k,j}$.

To obtain the unknowns $\hat{t}_{v,\mathrm{ex},k,i,j}$ and $\hat{C}_{k,i,j}$ from (19), the vehicle entry time to the crosswalk $t'_{v,\mathrm{en},k}$ is first determined for the hypothetical case of the vehicle being controlled in an open-loop manner based on the saturated linear speed trajectory shown in Fig. 10(a) (no Action 3 is considered)

$$t'_{v,\mathrm{en},k} = \begin{cases} |s_v(k)|/v_v(k), & \text{if } a_{v,R} = 0 \\ \dfrac{-v_v(k) + \sqrt{v_v^2(k) + 2a_{v,R}|s_v(k)|}}{a_{v,R}}, & \text{if } \Delta\hat{s} > |s_v(k)| \\ \Delta\hat{t} + \dfrac{|s_v(k)| - \Delta\hat{s}}{v_{v,R}}, & \text{if } \Delta\hat{s} \le |s_v(k)| \end{cases} \tag{20}$$

where $|s_v(k)|$ is the actual distance to the crosswalk, and $\Delta\hat{t}$ is the time instant of reaching the target speed $v_{v,R}$ (see Fig. 2), which is calculated as

$$\Delta\hat{t} = \left(v_{v,R} - v_v(k)\right)/a_{v,R}$$

and $\Delta\hat{s}$ is the corresponding traveled distance

$$\Delta\hat{s} = v_v(k)\,\Delta\hat{t} + a_{v,R}\Delta\hat{t}^2/2.$$

The second and third conditions in (20) relate to the case when the target distance $|s_v(k)|$ is reached prior and after getting to the target speed $v_{v,R}$, respectively [see Appendix, with emphasis on Fig. 15 and (26a)]. According to (9), the vehicle exit time $t'_{v,\mathrm{ex},k}$ is calculated by inserting the distance to the crosswalk trailing edge $|s_v(k)| + l_v$ in (20) instead of $|s_v(k)|$.

While iterating over all combinations of the pedestrian entry and exit time to evaluate (19), the following cases illustrated by the prediction horizon trajectories in Fig. 10 should be taken into account.

1) The vehicle enters the crosswalk prior to the pedestrian and no intervention of Action 3 is needed to prevent the collision [$t'_{v,\mathrm{en},k} \le \hat{t}_{p,\mathrm{en},k,i}$, Fig. 10(a)].
2) The pedestrian enters the crossing area prior to the vehicle and Action 3 is activated to prevent the potential collision [$t'_{v,\mathrm{en},k} > \hat{t}_{p,\mathrm{en},k,i}$, Fig. 10(b)].

In Case 1, the vehicle exit time and the collision flag are simply determined as

$$\begin{aligned} \hat{t}_{v,\mathrm{ex},k,i,j} &= t'_{v,\mathrm{ex},k} \\ \hat{C}_{k,i,j} &= 0, \quad \text{if } t'_{v,\mathrm{en},k} \le \hat{t}_{p,\mathrm{en},k,i}. \end{aligned} \tag{21}$$

In Case 2, the activation of Action 3 followed by Action 1 should be accounted for, as well. The acceleration under Action 3 is calculated based on the following expressions:

$$\hat{a}_v = \begin{cases} \dfrac{-\hat{v}_v^2\left(\hat{t}_{p,\mathrm{en},k,i}\right)}{2\left|\hat{s}_v\left(\hat{t}_{p,\mathrm{en},k,i}\right)\right|}, & \text{if } \hat{v}_{v,\max} < 0 \\ -\dfrac{\hat{v}_v\left(\hat{t}_{p,\mathrm{en},k,i}\right) - \hat{v}_{v,\max}}{\hat{t}_{p,\mathrm{ex},k,j} - \hat{t}_{p,\mathrm{en},k,i}}, & \text{if } 0 \le \hat{v}_{v,\max} \le \hat{v}_v\left(\hat{t}_{p,\mathrm{en},k,i}\right) \\ 0\ \dfrac{\mathrm{m}^2}{\mathrm{s}}, & \text{otherwise} \end{cases} \tag{22a}$$

$$\hat{v}_{v,\max} = \frac{2\left|\hat{s}_v\left(\hat{t}_{p,\mathrm{en},k,i}\right)\right|}{\hat{t}_{p,\mathrm{ex},k,j} - \hat{t}_{p,\mathrm{en},k,i}} - \hat{v}_v\left(\hat{t}_{p,\mathrm{en},k,i}\right) \tag{22b}$$

which correspond to the real Action 3 expressions (14) and (15), where the current vehicle position $s_v(k)$ and speed $v_v(k)$ are replaced with the ones projected to the time instant $\hat{t}_{p,\mathrm{en},k,i}$ of Action 3 activation, i.e., $\hat{s}_v(\hat{t}_{p,\mathrm{en},k,i})$ and $\hat{v}_v(\hat{t}_{p,\mathrm{en},k,i})$, respectively. Also, the pedestrian exit-to-entry time difference $\hat{t}_{p,\mathrm{ex},k}$ in (14) and (15) is replaced in (22) with the corresponding difference of polled entry and exit time, $\hat{t}_{p,\mathrm{ex},k,j} - \hat{t}_{p,\mathrm{en},k,i}$. Now, if the required deceleration $-\hat{a}_v(\hat{t}_{p,\mathrm{en},k,i})$ obtained by (22) is higher than its upper limit $a_{v,\max} = -a_{v,\min}$, the collision is

predicted to occur on the prediction horizon for the given set of control parameters

$$\hat{C}_{k,i,j} = \begin{cases} 1, & \text{if } \hat{a}_v\left(\hat{t}_{p,\text{en},k,i}\right) < a_{v,\min} < 0 \\ 0, & \text{otherwise.} \end{cases} \tag{23}$$

The vehicle traveling time $\hat{t}_{v,\text{ex},k,i,j}$ is then calculated by applying the piecewise-uniform acceleration-based equations derived in Appendix.

D. Computational Aspects

The proposed optimal control problem simplification based on only two control parameters (see Fig. 2), optimized via a grid-based approach, brings the execution time of Action 2 to the range from 1.5 to 2.5 s (when executed on a computer with Intel[1] Core[2] i7-7700HQ CPU at 2.80 GHz with 16-GB RAM installed). Although this execution speed is satisfying for virtual simulations, it would be too slow for real-time applications for the given sampling time of 0.1 s. Such a slow execution is due to the control strategy implementation within the MATLAB environment, which is known to be inefficient when dealing with a large number of custom iterations/loops (here, $N_{v_{v,R}} N_{a_{v,R,\text{abs}}} N^2 = 1.430.000$ grid search iterations in each sampling instant). Implementation within a compiled program (e.g., in C programming language) is expected to bring the execution time down by at least two orders of magnitude (i.e., to around 20 ms, see Cvok et al. [26]), which would make the strategy appropriate for real-time applications. The computational efficiency could be further improved by reducing the number of iterations, simply by omitting near-zero probability values of entry and exit time steps from iterations (see an example of probability distributions in Fig. 6, where most of the time steps have zero probability). More detailed consideration of computational and implementation aspects is a subject of future work.

VI. Simulation Results

A. Simulation Setup and Verification Metrics

The proposed safe speed control strategy has been verified against a Baseline control strategy (referred to as Baseline) by means of large-scale simulations. The Baseline strategy is based on replacing the Action 2-related SMPC block in Fig. 8 with forcing the vehicle to proceed with the initial speed $v_{v,0}$, while Actions 1 and 3 strategies remain unchanged for a fair comparison of the two strategies. The baseline strategy is set to be passive, i.e., nonreacting to the approaching pedestrian, in order to assess the relative benefits of the proposed safe speed control strategy operating proactively during the key Action 2.

In total, 300 simulations have been conducted for each of the two control strategies, where the initial conditions and the pedestrian model parameters are generated as described in Section III. Each simulation starts with Action 1 which is active until pedestrian appearance when Action 2 is activated. Action 3 is eventually activated if the pedestrian opts for crossing prior to the vehicle (see Fig. 8 and illustrations in Fig. 10). The main verification metrics include: 1) the actual vehicle traveling time $t_{v,\text{ex},0}$ (relative to the beginning of the simulation, $k = 0$); 2) the number of vehicle-pedestrian collisions [as defined by (10)]; and 3) the mean of nonzero decelerations $-a_v(k)$ occurring during the Action 3 interval, where a_v is calculated by (15b).

[1]Registered trademark.
[2]Trademarked.

TABLE II
Comparative Vehicle Traveling Time Statistics

Traveling time [s]	Baseline	SMPC
Mean	10.0	7.6
Median	8.7	7.2
Standard deviation	9.6	4.9

TABLE III
Statistics of Interaction Outcomes for Two Control Strategies Applied

Strategy	Vehicle prior to pedestrian	Pedestrian prior to vehicle	*Collision occurred
Baseline	162 (54.0%)	134 (44.7%)	4 (1.3%)
SMPC	193 (64.3%)	107 (35.7%)	0 (0.0%)

*Collision is identified according to definition (10).

B. Results

Fig. 12 shows the comparison of vehicle traveling time values obtained for the two control strategies. SMPC results in lower vehicle traveling time in a great majority of interactions when compared to Baseline control, i.e., more points are located below the unit line than above it [85% versus 15%, Fig. 12(a)]. Accordingly, the SMPC-related traveling time distribution is shifted toward lower values [see Fig. 12(b)], which is substantiated by the numerical values given in Table II. Furthermore, the SMPC application does not result in any collisions, while four collisions occur in the Baseline case (out of 300, i.e., 1.3%; Table III). It should be pointed out, however, that in real, complex environments characterized by a variety of pedestrian behaviors, one may expect situations in which actual pedestrian decisions/actions could differ significantly from model-based predictions, thus eventually resulting in collisions. To overcome the control strategy sensitivity to modeling errors, the SMPC strategy is proposed to be extended in [40] with a safety manifold, which prescribes additional distance-from-the-crosswalk-dependent vehicle velocity constraint to enable stopping in the case of pedestrian opting for crossing decision.

Fig. 13 shows the vehicle and pedestrian speed trajectories related to two collision cases designated as Examples 1 and 2 in Fig. 12. Baseline control keeps the initial vehicle speed and reacts through Action 3 braking only when the pedestrian enters the crosswalk. Due to the limited braking capability ($a_{v,\max} = 2$ m/s^2), the vehicle cannot stop on time, i.e., the collision occurs. On the other hand, SMPC persistently reduces the vehicle speed in Example 1 [see Fig. 13(a)] to account for the higher uncertainty of pedestrian crossing behavior. After the pedestrian eventually stops, the vehicle concludes that it is safe to accelerate and surpass the crosswalk prior

TABLE IV
STATISTICS RELATED TO ACTION 3 ACTIVATION

Strategy	No. of Action 3 activations	No. of brake applications	Mean positive deceleration during Action 3
Baseline	138 (46.0%)	11	1.75 m/s^2
SMPC	107 (35.7%)	15	0.725 m/s^2

to the pedestrian. In Example 2 [see Fig. 13(b)], where the pedestrian is initially more distant from the crosswalk and has a lower initial speed (see the figure legend), SMPC decides to fully accelerate to discourage the pedestrian from crossing and surpassing the crosswalk prior to him/her.

Table III shows the basic statistics of interaction outcomes for the two control strategies. When applying SMPC, the vehicle surpasses the crosswalk prior to the pedestrian in more cases than in the case of Baseline control (64.3% versus 54.0%), which is connected with the reduced traveling time, as observed in Table II and Fig. 12.

Furthermore, owing to anticipation of pedestrian behavior, Action 3 is activated less often for SMPC than Baseline control (35.7% versus 46.0% occasions, Table IV). Although the number of individual brake applications is somewhat higher for SMPC than for Baseline [note that activating Action 3 does not necessarily result in braking, see (15)], braking is much more aggressive in the latter case, thus significantly affecting the driving comfort (see Table IV). This is further illustrated through the vehicle speed trajectories shown in Fig. 14 for Action 3 conditions, which indicate that the maximum deceleration of 2 m/s^2 occurs in several Baseline cases, and not only those ending with collision. When compared to the Baseline case [see Fig. 14(a)], higher values of Action 3 initial speeds occur in the SMPC case [see Fig. 14(b)]. This indicates that SMPC often increases the vehicle speed through Action 2 to discourage the pedestrian from crossing the decision and thus achieve lower traveling time.

VII. CONCLUSION

This article has proposed a safe speed control strategy for AV when approaching unsignalized crosswalks with pedestrians. The proposed control strategy relies on 1) NN-based predictions of pedestrian behavior in terms of entry time to and exit time from the crosswalk and 2) SMPC aimed at minimizing the vehicle traveling time while keeping the probability of collision below the very low threshold.

It has been shown that the SMPC strategy outperforms the Baseline control strategy that tends to keep the initial vehicle speed. The improvement relates to the reduction of vehicle traveling time, number of pedestrian collisions, and discomfort (i.e., the strength of emergency deceleration applied through Action 3 control). More specifically, when compared to Baseline control, SMPC results in a) 24% lower traveling time on average, b) no collisions versus four collisions (out of 300 interactions), and reduced mean nonzero decelerations during Action 3 (0.725 versus 1.75 m/s^2).

The future work could be directed toward 1) extension of the proposed SMPC control strategy along with the NN prediction model to the multi-vehicle/multi-pedestrian scenario considered in [39] and pedestrians approaching the crosswalk from any direction; 2) its verification within a virtual simulation framework based on a more realistic, experimental data-driven stochastic pedestrian model recently proposed in [44]; 3) the strategy assessment against a) a globally optimal benchmark, which could be based on stochastic DP and Monte Carlo simulations and b) human driver-alike data-driven or game theory-based vehicle control; 4) implementation aspects regarding execution time minimization; and 5) development of a safety manifold to prevent any collisions that could eventually occur due to major pedestrian behavior prediction errors (see [40] for initial developments).

NOTATION

The variables related to pedestrian and vehicle are distinguished by indices p and v, respectively, with the position, speed, acceleration, probability-related, and time-related variables denoted as: s, v, a, p, and t. The predicted variables on the time horizon are distinguished from the actual/realized ones by hat symbol (e.g., $\hat{t}_{p,\mathrm{ex},k}$), while auxiliary variables are denoted with an apostrophe sign, e.g., a'_v. Indices containing en and ex refer to crosswalk entry and exit time instants. The time step index k denotes the current simulation/control time step, while i and j denote the future time steps on the prediction horizon related to the entry and exit time steps, respectively. For instance, $\hat{p}_{\mathrm{en},k,i}$ denotes the predicted probability of pedestrian entering the crosswalk at the time instant $\hat{t}_{p,\mathrm{en},k,i}$, corresponding to the ith time step on the horizon relative to the current kth time step.

APPENDIX

Calculating Vehicle Traveling Time: To determine the vehicle traveling time needed in (19), the following general equations of piecewise-uniform acceleration motion with speed saturation (as defined in Fig. 15) are introduced. They relate to position s_x and speed v_x at the given time instant t_x on the time horizon

$$s_x = \begin{cases} s_1 + v_1 t_x + a\dfrac{t_x^2}{2}, & \text{if } t_x < \Delta t \vee a = 0 \\ s_1 + v_1 \Delta t + a\dfrac{\Delta t^2}{2} + v_2\left(t_x - \Delta t\right), & \text{if } t_x \geq \Delta t \end{cases} \tag{24a}$$

$$v_x = \begin{cases} v_1 + a t_x, & \text{if } t_x < \Delta t \vee a = 0 \\ v_2, & \text{otherwise} \end{cases} \tag{24b}$$

where v_1 is the initial speed and Δt is the time instant of reaching the target speed v_2, which is given by

$$\Delta t = \left(v_2 - v_1\right)/a. \tag{24c}$$

Similarly, the position s_2 and the speed v_2 at the time instant Δt of purely accelerated motion read

$$v_2 = v_1 + a\Delta t \tag{25a}$$

$$s_2 = s_1 + v_1 \Delta t + a\Delta t^2/2. \tag{25b}$$

Furthermore, the time t_x needed to reach the target distance s_x (under the assumption of $s_1 = 0$) is obtained by solving (24a) as

$$t_x = \begin{cases} s_x/v_1, & \text{if } a = 0 \\ \left(-v_1 + \sqrt{v_1^2 + 2as_x}\right)\Big/a, & \text{else if } s_x < \Delta s \\ \Delta t + (s_x - \Delta s)/v_2, & \text{else if } s_x \geq \Delta s \end{cases} \tag{26a}$$

where Δs represents the distance traveled until reaching the target speed v_2

$$\Delta s = v_1 \Delta t + a\Delta t^2/2 \tag{26b}$$

where Δt is given by (24c).

Equations (24)–(26) are used below to determine the vehicle traveling time $\hat{t}_{v,\text{ex},k,i,j}$, for the presumed pedestrian entry ($\hat{t}_{p,\text{en},k,i} = i\Delta T$) and exit time values ($\hat{t}_{p,\text{ex},k,j} = j\Delta T$), the control parameters $v_{v,R}$ and $a_{v,R}$, and the case of the pedestrian entering the crosswalk prior to the vehicle ($\hat{t}_{p,\text{en},k,i} < t'_{v,\text{en},k}$, with $t'_{v,\text{en},k}$ given by (20); note that the traveling time for the alternative case of pedestrian entering the crosswalk after the vehicle is already covered by (21). In this case, the control actions are activated in the following order (see Fig. 16): Action 2, Action 3, and Action 1, where the quantities of interest are calculated for each of the corresponding time segments separately.

To obtain the vehicle position and speed at the time instant of pedestrian entry time, $\hat{t}_{p,\text{en},k,i}$, at the end of Action 2 on the prediction horizon (i.e., at the beginning of Action 3, see Fig. 16), the expression (24) is used, where the general variables given therein are replaced with the vehicle-related ones: $s_1 = s_v(k), v_1 = v_v(k), v_2 = v_{v,R}, a = a_{v,R}, t_x = \hat{t}_{p,\text{en},k,i}, s_x = \hat{s}_v(\hat{t}_{p,\text{en},k,i}), v_x = \hat{v}_v(\hat{t}_{p,\text{en},k,i})$.

Next, starting from the obtained values of vehicle position $\hat{s}_v(\hat{t}_{p,\text{en},k,i})$ and speed $\hat{v}_v(\hat{t}_{p,\text{en},k,i})$, the vehicle position and speed at the time instant of pedestrian exit time, $\hat{t}_{p,\text{ex},k,j}$, should be calculated. This is done based on the acceleration $\hat{a}_v(\hat{t}_{p,\text{en},k,i})$ obtained by (22) for hypothetical Action 3 activation, and by using (25) where the general variables are replaced with the vehicle-related ones as: $s_1 = \hat{s}_v(\hat{t}_{p,\text{en},k,i})$, $v_1 = \hat{v}_v(\hat{t}_{p,\text{en},k,i})$, $\Delta t = \hat{t}_{p,\text{ex},k,j} - \hat{t}_{p,\text{en},k,i}$, $a = \hat{a}_v(\hat{t}_{p,\text{en},k,i})$, $s_2 = \hat{s}_v(\hat{t}_{p,\text{ex},k,j})$, and $v_2 = \hat{v}_v(\hat{t}_{p,\text{ex},k,j})$. In the special case of $v_1 + a\Delta t < 0, v_2$ is saturated to zero ($v_2 = 0$) and s_2 equals to 0.

Finally, in the third, Action 1-related segment (see Fig. 16), the Action 1 acceleration $\hat{a}_v(\hat{t}_{p,\text{ex},k,j})$ is first calculated by substituting $v_v(k)$ with $\hat{v}_v(\hat{t}_{p,\text{ex},k,j})$ in (12). Then, (26) is used to determine the remaining time to the end of crosswalk, $\hat{t}_{\text{Act1}}$, where the general variables from (26) are replaced by the vehicle-related ones as: $v_1 = \hat{v}_v(\hat{t}_{p,\text{ex},k,j}), s_x = l_v + |\hat{s}_v(\hat{t}_{p,\text{ex},k,j})|, a = \hat{a}_v(\hat{t}_{p,\text{ex},k,j}), v_2 = v_{v,0}, t_x = \hat{t}_{\text{Act1}}$. Finally, the vehicle traveling time is obtained as

$$\hat{t}_{v,\text{ex},k,i,j} = \hat{t}_{p,\text{ex},k,j} + \hat{t}_{\text{Act1}}. \tag{27}$$

References

[1] A. Rasouli and J. K. Tsotsos, "Autonomous vehicles that interact with pedestrians: A survey of theory and practice," *IEEE Trans. Intell. Transp. Syst.*, vol. 21, no. 3, pp. 900–918, Mar. 2020.

[2] B. Völz, H. Mielenz, I. Gilitschenski, R. Siegwart, and J. Nieto, "Inferring pedestrian motions at urban crosswalks," *IEEE Trans. Intell. Transp. Syst.*, vol. 20, no. 2, pp. 544–555, Feb. 2019.

[3] D. Ridel, E. Rehder, M. Lauer, C. Stiller, and D. Wolf, "A literature review on the prediction of pedestrian behavior in urban scenarios," in *Proc. 21st Int. Conf. Intell. Transp. Syst. (ITSC)*, Maui, HI, USA, Nov. 2018, pp. 3105–3112.

[4] A. Rasouli, I. Kotseruba, T. Kunic, and J. Tsotsos, "PIE: A large-scale dataset and models for pedestrian intention estimation and trajectory prediction," in *Proc. IEEE/CVF Int. Conf. Comput. Vis. (ICCV)*, Oct. 2019, pp. 6261–6270.

[5] S. K. Jayaraman, L. P. Robert, X. J. Yang, A. K. Pradhan, and D. M. Tilbury, "Efficient behavior-aware control of automated vehicles at crosswalks using minimal information pedestrian prediction model," in *Proc. Amer. Control Conf. (ACC)*, Jul. 2020, pp. 4362–4368.

[6] N. R. Kapania, V. Govindarajan, F. Borrelli, and J. C. Gerdes, "A hybrid control design for autonomous vehicles at uncontrolled crosswalks," in *Proc. IEEE Intell. Vehicles Symp. (IV)*, Paris, France, Jun. 2019, pp. 1604–1611.

[7] S. Shalev-Shwartz, S. Shammah, and A. Shashua, "On a formal model of safe and scalable self-driving cars," 2017, *arXiv:1708.06374*.

[8] Y. Jeong, J. Yoo, Y. Yoon, and K. Yi, "Collision preventive velocity planning based on static environment representation for autonomous driving in occluded region," in *Proc. IEEE Intell. Veh. Symp. (IV)*, Jun. 2020, pp. 425–430.

[9] A.-T. Tran, A. Muraleedharan, H. Okuda, and T. Suzuki, "Scenario-based stochastic MPC for vehicle speed control considering the interaction with pedestrians," *IFAC-PapersOnLine*, vol. 53, no. 2, pp. 15325–15331, 2020.

[10] C. Nantabut and D. Abel, "A*-guided scenario-based stochastic model predictive control for an autonomous vehicle in simulated pedestrian environments," in *Proc. IEEE 25th Int. Conf. Intell. Transp. Syst. (ITSC)*, Macau, China, Oct. 2022, pp. 3472–3477.

[11] I. Batkovic, M. Zanon, M. Ali, and P. Falcone, "Real-time constrained trajectory planning and vehicle control for proactive autonomous driving with road users," in *Proc. 18th Eur. Control Conf. (ECC)*, Naples, Italy, Jun. 2019, pp. 256–262.

[12] J. Eilbrecht, M. Bieshaar, S. Zernetsch, K. Doll, B. Sick, and O. Stursberg, "Model-predictive planning for autonomous vehicles anticipating intentions of vulnerable road users by artificial neural networks," in *Proc. IEEE SSCI*, Honolulu, HI, USA, Nov. 2017, pp. 1–8.

[13] T. Rothermel, J. Pitz, and H.-C. Reuss, "Semi-autonomous longitudinal guidance for pedestrian protection in electric vehicles by means of optimal control," in *Proc. SAE Tech. Paper Ser.*, Detroit, MI, USA, Apr. 2016, pp. 1–8.

[14] Y. Jeong, S. Kim, and K. Yi, "Surround vehicle motion prediction using LSTM-RNN for motion planning of autonomous vehicles at multi-lane turn intersections," *IEEE Open J. Intell. Transp. Syst.*, vol. 1, pp. 2–14, 2020.

[15] C. Yuan et al., "Vehicle path planning based on pedestrian collision avoidance action," *IEEE Access*, vol. 11, pp. 66713–66728, 2023.

[16] R. Wang, M. Schuurmans, and P. Patrinos, "Interaction-aware model predictive control for autonomous driving," in *Proc. Eur. Control Conf. (ECC)*, Bucharest, Romania, Jun. 2023, pp. 1–6.

[17] T. Salzmann, B. Ivanovic, P. Chakravarty, and M. Pavone, "Trajectron++: Dynamically-feasible trajectory forecasting with heterogeneous data," in *Proc. 16th Eur. Conf. Comput. Vis. (ECCV)*, Glasgow, U.K. Cham, Switzerland: Springer, 2020, pp. 1–17.

[18] B. Varga, D. Yang, M. Martin, and S. Hohmann, "Cooperative decision-making in shared spaces: Making urban traffic safer through human-machine cooperation," in *Proc. IEEE 21st Jubilee Int. Symp. Intell. Syst. Informat. (SISY)*, Pula, Croatia, Sep. 2023, pp. 109–114.

[19] G. P. Rosati Papini, A. Plebe, M. D. Lio, and R. Dona, "A reinforcement learning approach for enacting cautious behaviours in autonomous driving system: Safe speed choice in the interaction with distracted pedestrians," *IEEE Trans. Intell. Transp. Syst.*, vol. 23, no. 7, pp. 8805–8822, Jul. 2022.

[20] A. Nagabandi, G. Kahn, R. S. Fearing, and S. Levine, "Neural network dynamics for model-based deep reinforcement learning with model-free fine-tuning," in *Proc. IEEE Int. Conf. Robot. Autom. (ICRA)*, May 2018, pp. 7559–7566.

[21] S. M. Thornton, B. Limonchik, F. E. Lewis, M. J. Kochenderfer, and J. C. Gerdes, "Toward closing the loop on human values," *IEEE Trans. Intell. Vehicles*, vol. 4, no. 3, pp. 437–446, Sep. 2019.

[22] S. M. Thornton, "Autonomous vehicle motion planning with ethical considerations," Ph.D. dissertation, Dept. Mech. Eng., Stanford Univ., Stanford, CA, USA, 2018.

[23] H. Bai, S. Cai, N. Ye, D. Hsu, and W. S. Lee, "Intention-aware online POMDP planning for autonomous driving in a crowd," in *Proc. IEEE Int. Conf. Robot. Autom. (ICRA)*, Seattle, WA, USA, May 2015, pp. 454–460.

[24] Z. Zhu and H. Zhao, "Learning autonomous control policy for intersection navigation with pedestrian interaction," *IEEE Trans. Intell. Vehicles*, vol. 8, no. 5, pp. 3270–3284, May 2023.

[25] B. Chen, D. Zhao, and H. Peng, "Evaluation of automated vehicles encountering pedestrians at unsignalized crossings," in *Proc. IEEE Intell. Vehicles Symp. (IV)*, Los Angeles, CA, USA, Jun. 2017, pp. 1679–1685.

[26] I. Cvok, L. Pavelko, B. Škugor, J. Deur, H. E. Tseng, and V. Ivanovic, "Design and comparative analysis of several model predictive control strategies for autonomous vehicle approaching a traffic light crossing," *Energies*, vol. 16, no. 4, pp. 1–20, Feb. 2023.

[27] P. Chen, C. Wu, and S. Zhu, "Interaction between vehicles and pedestrians at uncontrolled mid-block crosswalks," *Saf. Sci.*, vol. 82, pp. 68–76, Feb. 2016.

[28] B. Škugor, J. Topic, J. Deur, V. Ivanovic, and E. Tseng, "Analysis of a game theory-based model of vehicle-pedestrian interaction at uncontrolled crosswalks," in *Proc. Int. Conf. Smart Syst. Technol. (SST)*, Oct. 2020, pp. 73–81.

[29] B. Škugor, J. Deur, V. Ivanovic, and H. E. Tseng, "Stochastic model predictive control of an autonomous vehicle interacting with pedestrians at unsignalized crosswalks," in *Proc. Eur. Control Conf. (ECC)*, Bucharest, Romania, Jun. 2023, pp. 1–7.

[30] A. Tversky and D. Kahneman, "Advances in prospect theory: Cumulative representation of uncertainty," *J. Risk Uncertainty*, vol. 5, no. 4, pp. 297–323, Oct. 1992.

[31] L. Pavelko, B. Škugor, J. Deur, V. Ivanovic, and H. E. Tseng, "Modification and experimental validation of a logistic regression vehicle-pedestrian model," in *Proc. Int. Conf. Smart Syst. Technol. (SST)*, Oct. 2022, pp. 109–114.

[32] J. Bock, R. Krajewski, T. Moers, S. Runde, L. Vater, and L. Eckstein, "The inD dataset: A drone dataset of naturalistic road user trajectories at German intersections," in *Proc. IEEE Intell. Vehicles Symp.*, Las Vegas, NV, USA, Oct. 2020, pp. 1929–1934.

[33] J. Topic, B. Skugor, J. Deur, V. Ivanovic, and H. E. Tseng, "Neural network-based prediction of pedestrian crossing behavior at unsignalized crosswalks," in *Proc. Int. Conf. Smart Syst. Technol. (SST)*, Oct. 2022, pp. 101–107.

[34] I. Goodfellow, J. Bengio, and A. Courville, *Deep Learning*. Cambridge, MA, USA: MIT Press, 2016.

[35] *Keras*. Accessed: Apr. 24, 2025. [Online]. Available: https://keras.io

[36] *Tensorflow*. Accessed: Apr. 24, 2025. [Online]. Available: https://tensorflow.org

[37] D. P. Kingma and J. Ba, "Adam: A method for stochastic optimization," in *Proc. 3rd Int. Conf. Learn. Represent.*, San Diego, CA, USA, 2015, pp. 1–15.

[38] M. Ćorić, B. Skugor, J. Deur, V. Ivanovic, and H. E. Tseng, "Hierarchical neural network-based prediction model of pedestrian crossing behavior at unsignalized crosswalks," in *Proc. SAE Tech. Paper Ser.*, vol. 1, Apr. 2023, pp. 1–13.

[39] L. Pavelko, B. Škugor, J. Deur, V. Ivanovic, and H. E. Tseng, "Game theory-based modeling of multi-vehicle/multi-pedestrian interaction at unsignalized crosswalks," in *Proc. SAE Paper*, 2022, pp. 1–9.

[40] B. Škugor, J. Deur, V. Ivanović, and H. E. Tseng, "Safety manifold for stochastic model predictive control of an autonomous vehicle approaching unsignalized crosswalks with pedestrians," in *Proc. Int. Conf. Smart Syst. Technol. (SST)*, Osijek, Croatia, Oct. 2024, pp. 279–285.

[41] V. S. Raković and W. S. Levine, *Handbook of Model Predictive Control*. Cham, Switzerland: Springer, 2019, p. 692.

[42] T. Brüdigam, F. D. Luzio, L. Pallottino, D. Wollherr, and M. Leibold, "Grid-based stochastic model predictive control for trajectory planning in uncertain environments," in *Proc. IEEE 23rd Int. Conf. Intell. Transp. Syst. (ITSC)*, Sep. 2020, pp. 1–8.

[43] D. R. Jones, C. D. Perttunen, and B. E. Stuckman, "Lipschitzian optimization without the Lipschitz constant," *J. Optim. Theory Appl.*, vol. 79, no. 1, pp. 157–181, Oct. 1993.

[44] Z. Dabčević, B. Škugor, J. Deur, V. Ivanović, and H. E. Tseng, "Stochastic neural network-based modeling of pedestrian crossing behavior at unsignalized crosswalks," *IEEE Trans. Intell. Transp. Syst*, to be published.

Branimir Škugor (Member, IEEE) received the Ph.D. degree in mechanical engineering from the University of Zagreb, Zagreb, Croatia, in 2016.

He is currently an Assistant Professor with the University of Zagreb. He has participated in numerous projects supported by Croatian Science Foundation, European Commission, and Ford Motor Company. His research interests include advanced controls of hybrid electric vehicle powertrains, modeling and charging optimization of electric vehicle fleets, synthesis of driving cycles, machine learning with automotive applications, and autonomous vehicle control.

Jakov Topić received the Ph.D. degree in mechanical engineering from the University of Zagreb, Zagreb, Croatia, in 2022.

He is a Software Developer at dSPACE Engineering d.o.o. His research interests include the synthesis of multidimensional driving cycles, road transport electrification planning, and artificial intelligence in automotive and traffic systems.

Joško Deur (Senior Member, IEEE) is a Full Professor at the University of Zagreb, where he teaches courses in electrical machines and servodrives, digital control systems, automotive mechatronics, and electric vehicle controls. In 2000, he was a Guest Researcher at the Ford Research Laboratory, Dearborn, MI. He has led numerous projects including those supported by Ford Motor Company and Jaguar Cars Ltd. His main research interests include modelling and control of automotive mechatronic systems and electric vehicles.

Vladimir Ivanovic received the Ph.D. degree in mechanical engineering from the University of Zagreb, Zagreb, Croatia, in 2010.

He is a Technical Leader for Motion Controls in ADAS Technologies at Ford Motor Company. Since he joined Ford Motor Company in 2011, he has contributed to a number of research and production vehicle implementation applications in the area of automatic transmissions, active drivelines, and advanced driver assistance systems. His research interests include modeling and control of automotive systems.

Dr. Ivanovic's technical achievements at Ford have been recognized with two Ford's highest technical awards and the Henry Ford Technical Fellow.

H. Eric Tseng received the B.S. degree from the National Taiwan University, Taipei, Taiwan, in 1986, and the M.S. and Ph.D. degrees in mechanical engineering from the University of California at Berkeley, Berkeley, CA, USA, in 1991 and 1994, respectively.

In May 2024, he joined The University of Texas at Arlington, Arlington, TX, USA, as a Distinguished University Professor with the Department of Electrical Engineering. In 1994, he joined Ford Motor Company, Dearborn, MI, USA. At Ford (1994–2022), he had a productive career and retired as a Senior Technical Leader of controls and automated systems with Research and Advanced Engineering. Many of his contributed technologies led to production vehicle implementation. He has over 100 U.S. patents and over 160 publications.

Dr. Tseng is a member of the National Academy of Engineering (2021). His technical achievements have been honored with Ford's Annual Technology Award, the Henry Ford Technology Award, on seven occasions. In addition, he was a recipient of the Control Engineering Practice Award from American Automatic Control Council in 2013 and the Soichiro Honda Medal from American Society of Mechanical Engineering in 2024.